Arch. Metall. Mater. **69** (2024), 4, 1501-1508

DOI: https://doi.org/10.24425/amm.2024.151420

T. AYDIN[1*], H. SARI[2]

THE EFFECTS OF CaO AND MgO ON THERMAL, MECHANICAL AND OPTICAL PROPERTIES OF PORCELAIN TILES BY UTILIZING BLAST FURNACE SLAG

In this study, the Blast Furnace Slag (BFS) of Zonguldak Eregli Iron and Steel Factories was used as a recycling raw material for the porcelain tile samples. A kind of clay with high MgO content was also used in the porcelain tile recipes. Maximum 10% of BFS was used instead of Na-feldspar. Sintering temperature for all samples was 1205°C for 50 minutes in the industrial roller kiln. Technological properties such as shrinkage, water absorption, colour measurement, and flexural strength were investigated as well as sintering properties and microstructures of the green and the sintered samples. As a result of the study, the addition of BFS did not adversely affect the technical properties of porcelain tile bodies. Particularly, the addition of BFS up to 3% contributed to an increase in flexural strength, and whiteness values of all samples increased because of the formation of anorthite and diopside compared to the reference body. The phase transformations and crystal formations such as anorthite and diopside resulted in a decrease in the firing shrinkage. Although the anorthite formation and diopside formation in the investigated samples had an adverse effect on condensation, it was found that they showed similar sintering behaviours compared to the reference body. This study showed that an industrial waste material can be converted into an environmentally friendly raw material that can create added value and provide energy efficiency.

Keywords: Porcelain tile; sintering; anorthite; diopside; whiteness; recycling

1. Introduction

Unwanted by-products and industrial scraps from factory processes should not be considered wastes. They are actually an unused alternative raw material source [1]. The undeniable economic value of the products is neglected because they are constantly associated with the negative aspects of the environment [2]. Reusing of these materials as an alternative raw material is crucial both for the economy and for the environmental management. Because natural raw material resources are becoming increasingly depleted and raw material costs are increasing rapidly. This situation forces manufacturers to use low-quality raw materials. One of the challenges of using waste materials is that they are currently considered "wasted" materials. One of the first steps to overcoming this challenge will be to understand the nature of industrial and post-consumer waste. Porcelain tiles are commonly produced using clay, kaolin, feldspars, and quartz. The most important technical properties of porcelain tiles are low water absorption (0.5% ≤) and almost zero open porosity. These raw materials contain SiO_2, Al_2O_3, Na_2O, K_2O, CaO and MgO. Since Blast Furnace Slag (BFS) contains all these oxides, it is a good alternative raw material source for porcelain tile production. In the literature, there are lots of studies on waste materials used as alternative raw materials [3-5]. Many authors have shown the beneficial aspects of BFS in the production of ceramic materials. BFS addition at a rate of 33% resulted in about a 25% increase in bending strength [6]. It was shown that unglazed ceramic tiles could be made from BFS [7]. In another study, the granulated BFS was used. They found that optimum compositions were found as 0.1-0.3 for the $CaO\text{-}SiO_2$ ratio [8]. Most of the studies in the literature are related to mechanical properties and microstructure. Alkali earth and alkaline oxides are traditional glass network modifiers. They result in the formation of non-bridging oxygen sites. Also, all of them reduce the viscosity in the glass melting range [9]. If an alkali ion is substituted by another alkali ion, the glass properties show non-linear behaviours they are depending on the mobility of the modifier ions such as Na^+ and K^+. This non-linear behaviour is mostly related with the viscous flow. This situation is named as Mixed Alkaline Effect. The addition of alkaline-earth modifiers (Mg^{+2},

[1] KIRIKKALE UNIVERSITY, ENGINEERING FACULTY, METALLURGY AND MATERIAL ENGINEERING DEPARTMENT, KIRIKKALE, TURKEY
[2] KALE SERAMIK CANAKKALE KALEBODUR SERAMIK SAN. A.S. CANAKKALE, TURKEY
* Corresponding author: tunaaydin@kku.edu.tr

Ca^{+2}) may affect the mixed alkaline effect. This phenomenon is called as "Mixed Alkaline-Earth Effect [9]. Mixed Alkaline-Earth Effect" affects both the technical and thermal properties of ceramic materials [6].

In this study, the effects of BFS on the thermal, mechanical, and optical properties of porcelain tiles were investigated. In particular, the results obtained on optical properties (opacity and whiteness) were the most important results of the present study.

2. Material and methods

In this study, the batch composition of an industrial porcelain tile was selected as the Reference (RF) composition. An X-ray fluorescence analyser was used to determine the chemical compositions of the raw materials (Panalytical Axios XRF, Kale Ceramic Research Centre). After the grinding process, the sieve residue of granules under 63 μm is below 0.06%. All dried granules were pressed using a uniaxial press in a 5 cm×10 cm steel mold at 320 kg/cm^2. Drying was conducted at about 110°C. The firing process was performed in a roller kiln at 1205°C for 50 minutes in Kale Ceramic. The firing of the samples was carried out in an oxygen atmosphere. The colour measurement of the bodies was conducted using a colour measuring instrument (Minolta Konica, 3600d colorimeter, Kale Ceramic Research Centre). The color parameters such as the lightness (L), and a^* and b^* color values were measured. A non-contact optical dilatometer was used in order to determine the sintering behaviour (Netzch 402 EP dilatometer, Kale Ceramic Research Centre). First, green bodies were heated up to 500°C with 80°C/min intervals. All samples were heated up to 1300°C with 50°C/min intervals. The phase analyses of the sintered samples were conducted by X-ray diffractometer (XRD) (Panalytical X' Pert Pro MPD diffractometer, Kale Ceramic Research Centre). Samples were scanned from 3° to 70° with 2°/min intervals. A scanning Electron Microscope (SEM) was used to observe the microstructures of the bodies by using backscattered electrons (SEM, Zeiss EVO 50EP, Ceramic Research Centre, Turkey). The polished surfaces were prepared and then, the etching process was performed for 2 min in a 5% HF solution. Then, samples were coated with Au and Pd to perform the SEM-EDX analysis. The bulk densities of the samples were measured using a Helium Pycnometer (Quantachrome, MVP-1 Multipycnometer). Water absorption of sintered samples was measured according to ISO-EN 10545-3 standards. Samples were weighted before boiling (M5), weighted after boiling 4 h and waiting for 2 h (M15). Water absorption was calculated according to Eq. (1) as follows:

$$\text{Water absorption (W.T.) \%} \left(\frac{m_2 - m_1}{m_1} \right) \times 100 \qquad (1)$$

2.1. Preparing of body compositions

All samples were prepared under industrial conditions in Kale Ceramic. Bodies were composed of kaolin, sodium feldspar, two types of clay, and magnesite called magnesite clay composed of a high amount of $MgCO_3$. Blast Furnace Slag (BFS) was used as CaO and MgO. In this study, BFS that was obtained from Zonguldak Eregli Iron and Steel plants was used. BFS was substituted by sodium feldspar in the Reference Body (RF) at rates of 1%, 3%, 5%, and 10%. The chemical analyses of the raw materials are given in TABLE 1. The BFS used in this study contained 36.55% CaO and 4.82% MgO.

2.2. Phase Analysis (XRD)

The XRD analyses of the fired samples are given in Fig. 1. The Reference Body (RF) contained quartz, mullite, albite and glassy phase. With the addition of BFS, anorthite ($CaO.Al_2O_3.2SiO_2$) and pigeonite phases formed. PTBF1, PTBF2, PTBF3, and PTBF4 bodies contained quartz, mullite, anorthite and, diopside-alumina. As the addition of BFS continued to increase, anorthite and diopside-alumina peaks intensity began to increase, and albite, and glassy phase intensity began to decrease. The formation of anorthite ($CaO.Al_2O_3.2SiO_2$) crystals occurs from metakaolinite ($Al_2O_3.2SiO_2$) [10]. The diopside and anorthite crystals start to form at a temperature from 700°C to 800°C. BFS contributes high CaO composition and provides crystallization at low temperature. The formation of the akemantite phase ($Ca_2Mg(Si_2O_7)$ occurs at approximately 900°C. At approximately 1000°C, akemantite transforms into diopside, and increases the amount of diopside. At about 1000°C, the formation of andradite ($Ca_3Fe_2(SiO_4)_3$) from BFS occurs. Above 1150°C, the andradite phase begins melting, and the diopside phase transforms into the diopside-alumina phase ($Mg_{0.851}Fe_{0.026}Al_{0.080}Ti_{0.003}Cr_{0.040}$) ($Ca_{0.720}Na_{0.027}Mg_{0.179}Fe_{0.071}Mn_{0.003}$) ($Si_{1.891}Al_{0.109}$)$O_6$. Above 1200°C, anorthite and quartz begin

TABLE 1

Chemical Analyses (XRF)

	Lol	SiO_2	Al_2O_3	Fe_2O_3	TiO_2	CaO	MgO	Na_2O	K_2O	Mn_3O_4	SO_3
Clay A	7.07	64.86	22.56	1.43	0.94	0.16	0.38	0.18	2.27	—	—
Clay B	8.19	58.61	22.04	5.68	1.38	0.27	0.87	0.18	2.60	—	—
Magnesite	45.68	8.88	1.81	0.37	0.23	1.29	40.94	0.21	0.10	—	—
Na Feldspar	0.38	71.91	16.9	0.09	0.18	0.53	0.16	9.35	0.25	—	—
Kaolin	7.70	70.50	20.73	0.38	0.47	0.02	0.03	0.10	0.05	—	—
BFS	0.47	40.39	11.82	0.77	1.07	36.55	4.82	0.28	0.93	1.11	—

Lol: loss on ignition

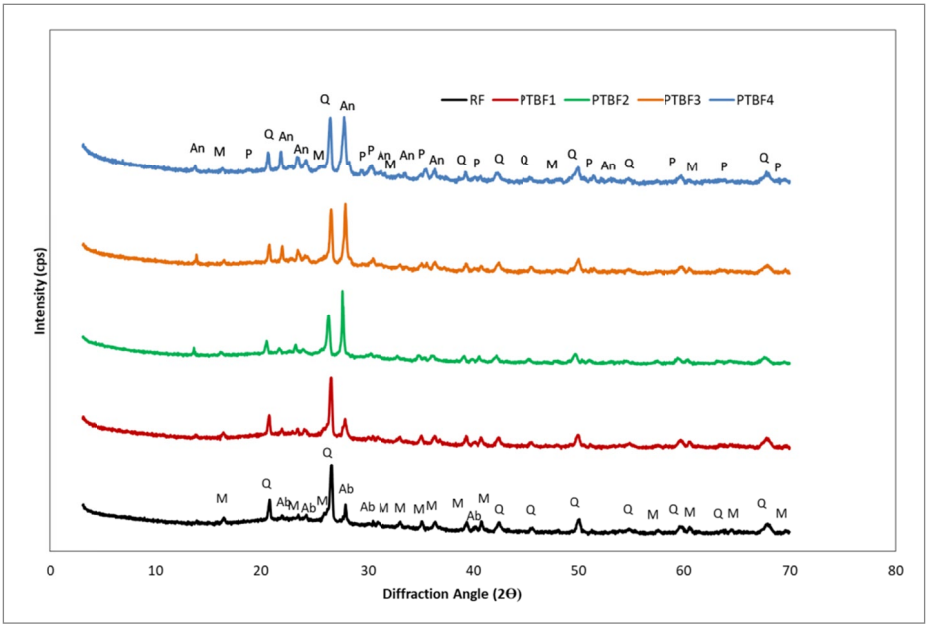

Fig. 1. XRD curves of sintered samples; Ab: Albite, Q: Quartz, An: Anorthite, M: Mullite, P: Diopside-alumina

TABLE 2

Technological Properties of the samples

		RF	PTBF1	PTFB2	PTBF3	PTBF4
Green density(g.cm^{-3})		1.93	1.98	1.99	1.97	1.95
Bulk density (g.cm^{-3})		2.41	2.11	2.34	2.34	2.30
Water absorption (%)		0.00	0.05	0.01	0.01	0.02
Green strength (N.mm^{-2})		3.00	3.20	4.10	3.60	3.20
Flexural strength (N.mm^{-2})		68.5	70.2	71.6	69.7	64.9
Colour measurement	L	61.89	63.45	63.32	62.02	64.81
	a*	2.02	2.07	1.62	1.67	1.56
	b*	12.59	13.74	13.45	13.61	14.92
Grain size distribution (+45 µm)		1.60	1.48	1.48	1.56	1.44
Firing shrinkage (%)		7.75	6.30	6.21	6.06	5.01

melting, and diopside-alumina forms [11]. Diopside-alumina contains iron brought by kaolin and BFS. Iron enters the lattice of diopside crystals through a solid-state reaction [12,13]. As can be seen in TABLE 2, the higher whiteness of bodies containing BFS resulted from the diffusion of iron ions into the diopside lattice. This prevented the formation of FeO4 tetrahedrons in the glassy phase. Thus, the whiteness values of the fired samples increased [12,13]. As mentioned before, the glassy phase content decreased with the addition of BFS, which contributed to obtaining higher bending strength.

2.3. Technological Properties

The bulk densities of the samples were measured using a Helium Pycnometer. In this study, the density of bodies containing BFS was low as 2.11-2.34 g/cm^{-3} compared to the RF body (2.41 g.cm^{-3}). The specific values of the bulk density of porcelain tiles should not be under 2.00 g/cm^3. One of the reasons for this decrease was the formation of anorthite crystals (2.76 g.cm^{-3}). Anorthite has a much lower density than mullite crystals (3.16 g.cm^{-3}) [12,13]. The other reason was related to sintering kinetics. As seen in Fig. 1, a large amount of anorthite and diopside crystals formed in the bodies containing BFS. Crystal formations result in a decrease in the firing shrinkage and have an adverse effect on densification [14]. This resulted in a decrease in bulk density and firing shrinkage. The decrease in bulk density is also responsible for increase in water absorption. The specific value of the water absorption of the porcelain tiles is 0.5%. The flexural strength of the bodies containing BFS is higher than the reference body except for PTBF4. The increase in the strength is related to both second phase addition and a lower amount of glassy phase [15-18]. The formation of anorthite and diopside contributed to obtaining higher strength up to 3% of BFS (PTBF2). It also contributed to the lower glassy phase. However, the addition of a higher amount of BFS (10% wt.) affected flexural strength negatively due to lower mullite content. The main mechanism of strength in porcelain is the Mullite Hypothesis, which reveals that the interlocking of fine mullite needles is directly responsible for the strength

of a porcelain body [15-18]. The whiteness (L) of the samples containing BFS was higher than that of the Reference Body because crystalline calcium-silicates had an opacifying effect so diopside and anorthite increased the L values of porcelain tile bodies [10]. Also, as mentioned in section 2.2, the iron diffusion into the diopside lattice contributes to obtaining higher whiteness values for bodies containing BFS. The firing shrinkage values of PTBF1, PTBF2, PTBF3, and PTBF4 were lower than the RF due to the anorthite and diopside-alumina crystallization during sintering [14]. Green density and green strength values were higher than the RF body. The increase in green density and green strength is an important result that will contribute to the reduction of production losses.

2.4. Thermal properties

Fig. 2 presents the linear shrinkage (%) on the function of temperature and time during the firing process. The sintering curves show that the RF body had a significantly higher firing shrinkage than the bodies containing BFS. These data are very close to the firing shrinkage values in TABLE 2. As mentioned in section 2.3, this was due to anorthite and diopside-alumina crystallization during sintering. In the literature, it was explained that the phase transformations and crystal formations result in a decrease in the firing shrinkage. The phase transformations and crystal formations have an adverse effect on densification [14]. As seen on sintering curves, there was a slight volume expansion due to quartz transformation. After the quartz transformation, there was a sharp drop due to the sintering shrinkage. The flex temperature shows the temperature of the highest sintering rate. The flex temperature of the RF body was 1190°C. However, the sintering rate reached the highest rate at 1175°C, 1180°C, 1177°C, and 1200°C, respectively for PTBF1, PTBF2, PTBF3, and PTBF4 samples. It was determined that as the amount of BFS increased, the flex temperature of the samples decreased, except for PTBF4. This shows that bodies containing BFS up to a rate of 10% can be sintered at a lower temperature. As mentioned before, when crystallization occurs during sintering, the sintering rate decreases. Sintering is restricted, and a completely or partially crystallized porous body is obtained, if the crystallization ™present on the entire surface [19,20]. As seen in Fig. 2, the shrinkage is a function of temperature during constant heating rate in the sintering process. A slope, *dy*/*dT*, can be calculated from such a curve. The dy/dT values show the sintering rate. The *dy*/*dT* values of all samples are given in TABLE 3. As mentioned before, crystallization resulted in a decrease in the sintering rate.

TABLE 3

dy/*dt* values of samples

	$dy/dT \times (10^{-3})$
RF	45.04
PTFB1	40.06
PTFB2	39.77
PTFB3	32.35
PTFB4	33.26

2.5. Microstructure (SEM)

The images of SEM and EDX of all samples are given in Fig. 3a, Fig. 4a, Fig. 5a, Fig. 6a and Fig. 7a. Fig. 3 shows the microstructure of the Reference (RF) body. The needle and cuboidal crystals were found in the microstructure. These crystals are determined as primary and secondary mullite crystals [6]. Quartz and glassy phase were also observed in the RF body.

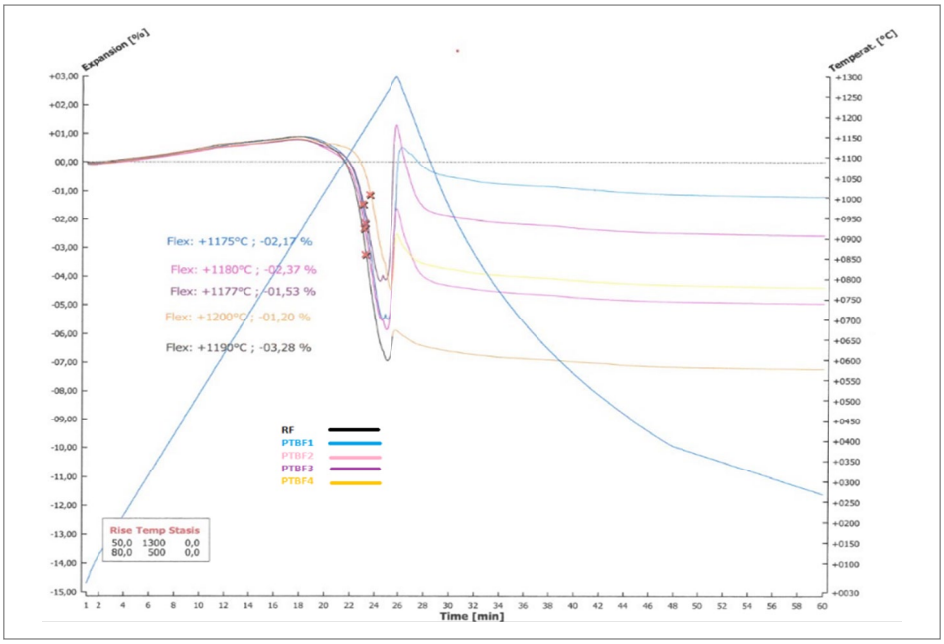

Fig. 2. Sintering curves of RF, PTBF1, PTBF2, PTBF3, and PTBF4 bodies

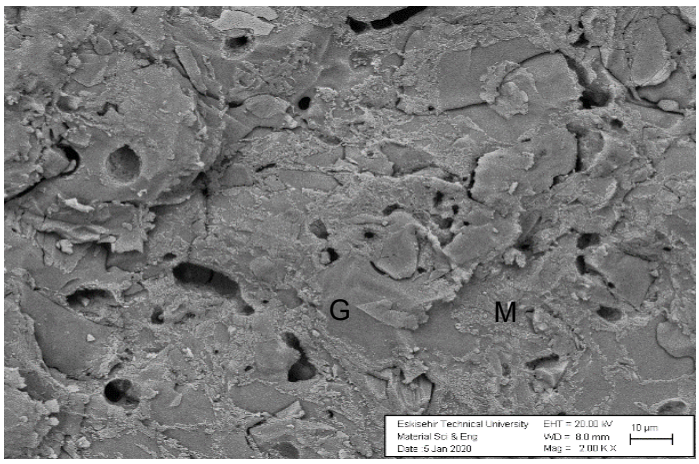

Fig. 3a. Microstructure image of the RF body, G: Glassy phase, M: Mullite

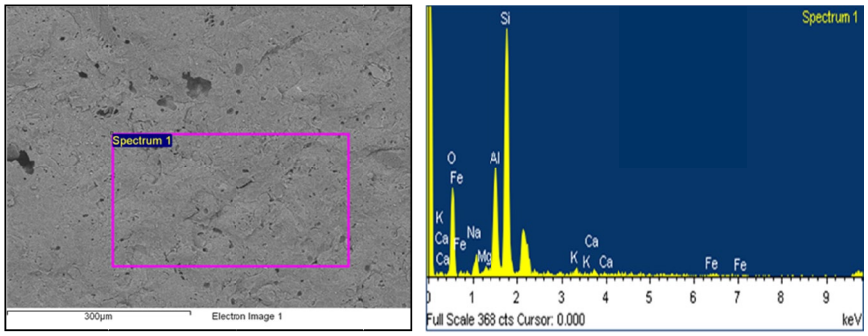

Fig. 3b. EDX images of the RF body

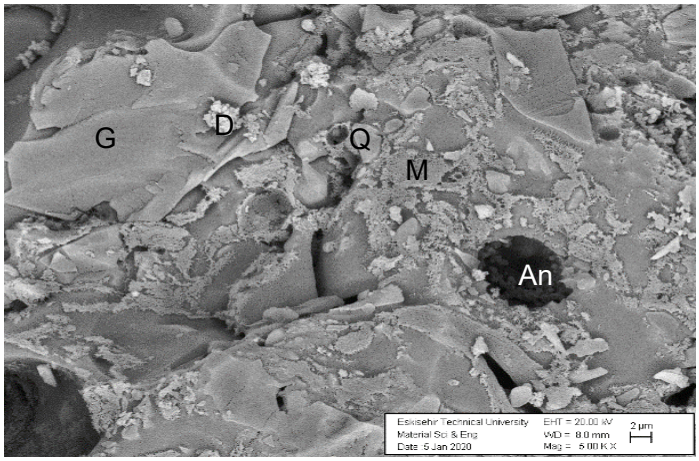

Fig. 4a. Microstructure image of PTBF1 body. G: Glassy phase, M: Mullite, Q: Quartz, An: Anorthite, D: Diopside

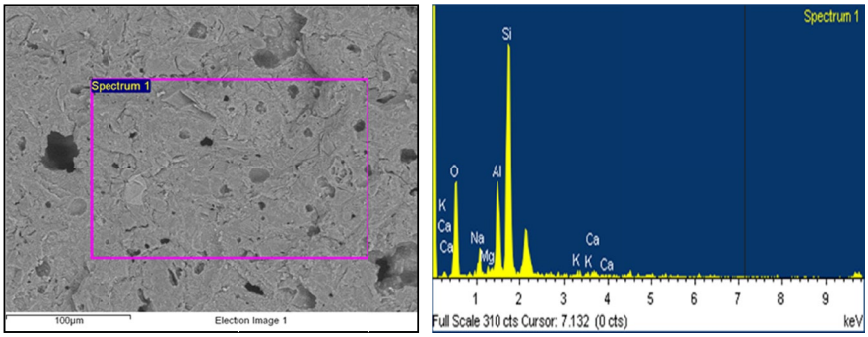

Fig. 4b. EDX images of PTBF1 body

According to the EDX analysis, a large amount of Fe_2O_3 was also determined.

The images of the microstructure and EDX of the PTBF1 body are given in Fig. 4. Primary and secondary mullite crystals, quartz, and glassy phase were determined in this respect. The crystals of diopside and anorthite were also detected. These crystals seen as spherical and white in microstructure are anorthite crystals [6]. According to the EDX analysis of the PTBF1 body, Fe_2O_3 was eliminated. As mentioned before, iron enters the lattice of diopside crystals through a solid-state reaction [12,13]. This yielded higher whiteness values than the RF body.

Fig. 5a shows the microstructure and EDX images of the PTBF2 body. As seen in Fig. 5a, the needle and cuboidal mullite and quartz crystals were determined in the microstructure. Large amounts of anorthite and diopside crystal were also detected embedded in the glassy phase and pores. As mentioned for the PTBF1 body, Fe_2O_3 was eliminated in the PTBF2 body due to the iron entering the lattice of diopside crystals.

Fig. 6a and Fig. 7a show the microstructure and EDX images of the PTBF3 and PTBF4 body. Compared to the structure of PTBF1 and PTBF2, PTBF3 and PTBF4 have very high anorthite and diopside crystals. It can also be seen from the microstructure images that the mullite crystals decreased compared to the PTBF1 and PTBF2 structures. This situation shows the reason for the decrease in strength in PTBF3 and PTBF4 bodies. As seen in EDX analyses of the bodies, similar to PTBF1 and PTBF2 bodies, iron oxide was also eliminated by trapping within the diopside structure in PTBF3 and PTBF4. A large amount of porosity formed in the PTBF2 body, because the increase in crystallization resulted in a decrease in the sintering rate.

3. Conclusion

The recycling of waste materials has a big potential to provide significant gains to manufacturers both in economic terms and for environmental management. In this context, the results obtained in this study are important because industrial waste was used as a ceramic raw material in it. The present study shows that optical properties such as whiteness that can be only obtained with pure and expensive raw materials (alumina and zircon) can also be achieved by using waste materials. This finding is the most important result of the study. The diffusion of iron ions into the diopside lattice was responsible for the higher whiteness in the bodies containing Blast Furnace Slag. This prevents the formation of FeO_4 tetrahedrons in the glassy phase. Thus, the whiteness values of the fired samples increased. This finding suggested that, for future studies, Blast Furnace Slag and magnesite named magnesium clay could be used instead of alumina and zircon, which have high costs in obtaining high whiteness in super white bodies. With the use of Blast Furnace Slag, green densities and green strengths also increased. This will ultimately lead to a reduction in production costs and reduce production

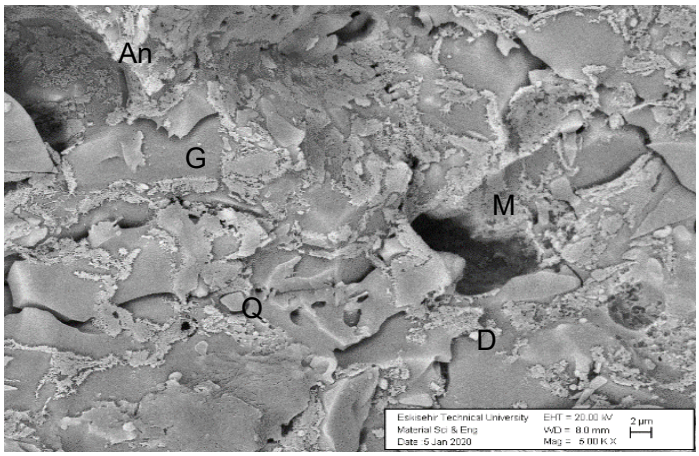

Fig. 5a. Microstructure image of PTBF2 body. G: Glassy phase, M: Mullite, An: Anorthite, D: Diopside, Q: Quartz

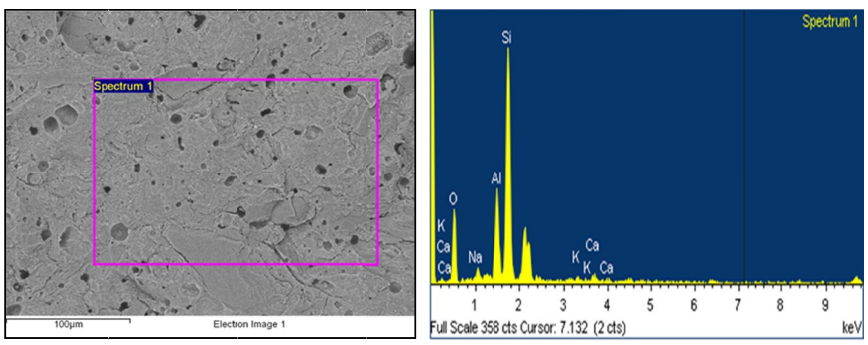

Fig. 5b. EDX images of PTBF2 body

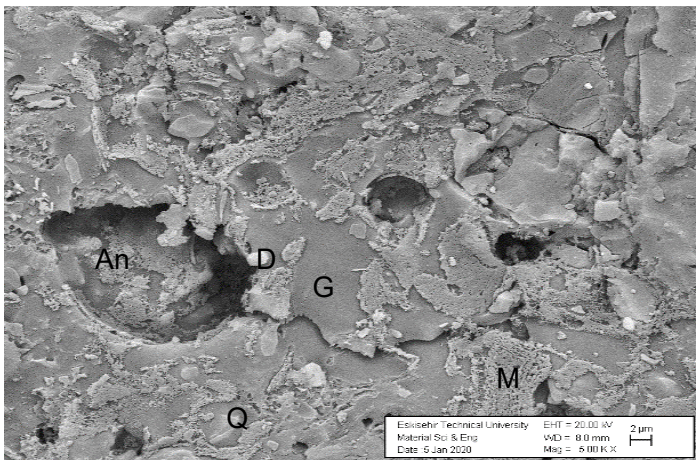

Fig. 6a. Microstructure and EDX images of PTBF3 body. G: Glassy phase, M: Mullite, Q: Quartz, An: Anorthite, D: Diopside

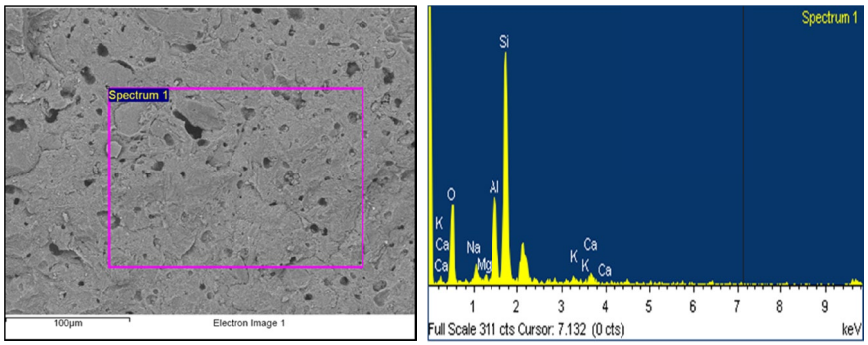

Fig. 6b. Microstructure and EDX images of PTBF3 body

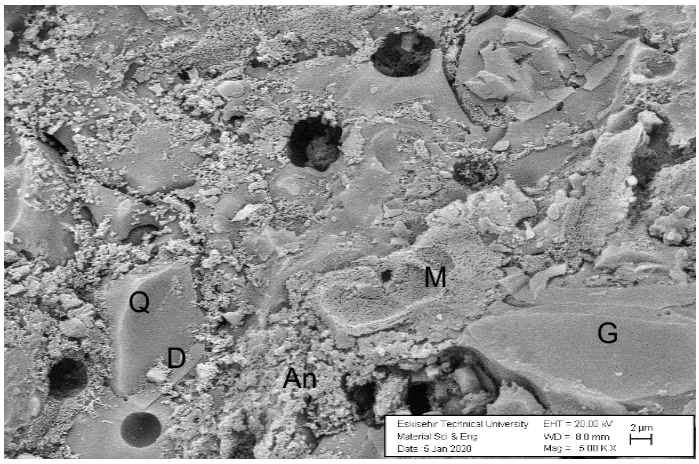

Fig. 7a. Microstructure and EDX images of PTBF4 body. G: Glassy phase, M: Mullite, Q: Quartz, An: Anorthite, D: Diopside

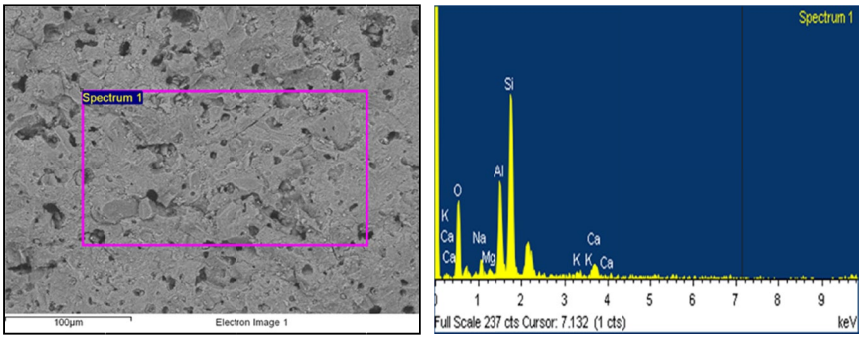

Fig. 7b. Microstructure and EDX images of PTBF4 body

losses. As the amount of Blast Furnace Slag increased up to 10%, the flex temperature of the samples decreased. This shows that the bodies containing Blast Furnace Slag up to 10% can be sintered at a lower temperature compared to the Reference body. This is an important finding in terms of reducing energy costs. As a result, this study showed that industrial waste material can create a new added value, provide energy efficiency, and can be turned into an environmentally friendly raw material.

Acknowledgements

The authors would like to thank Kale Seramik A.S.

REFERENCES

[1] D.T. Allen, N. Behmannesh, National Academy Press. 69-89. https://www.nap.edu/read/2129/chapter/7 (1994).

[2] R.G. Popa, L.G. Popescu, T.A. Abagiu, C. Popescu, R. Cazalbasu, Metalurgija **54**, 1, 297-300 (2015).

[3] B. Tarhan, Journal of the Australian Ceramic Society **55**, 737-746 (2019).

[4] B. Tarhan, M. Tarhan, T. Aydin, Ceramics International **43**, 3, 3107-3112 (2017).

[5] M. Tarhan, B. Tarhan, T. Aydin, Ceramics International **42**, 15, 17110-17115 (2016).

[6] Z.B. Ozturk, E.E. Gultekin, Ceram. Int. **41**, 12020-12026 (2015).

[7] I. Ozdemir, S. Yılmaz, J. Mater. Proc. Tec. **183** (1), 13-17 (2007).

[8] S. Ghosh, M. Das, S. Chakrabarti, Ceram. Int. **28**, 393-400 (2002).

[9] T. Aydin, E. Casin, Waste and Biomass Valorization **12**, 2685-2702 (2021)

[10] S.J.G. Sousa, J.N.F. Holanda. https://pdfs.semanticscholar.org/cf62/df00fbd63e337ec8b489210b1929e010ad7b.pdf

[11] L. Zhao,Y. Li, L. Zhang, D. Cang, ISIJ International **57** (1), 15-22 (2017).

[12] J. Wu, K. Li, X. Xu, Y. Zhang, X. Xu, X. Lao, Int. J. Appl. Ceram. Technol. **14**, 454-460 (2017).

[13] F. Kara, M. Cava, Qualicer 2002, Catelion, Spain (2002).

[14] M. Tarhan, J. Therm. An. Calori. **138**, 929-936 (2019).

[15] L. Vodova, R. Sokolar, J. Hroudova, International Journal of Civil, Environmental, Structural, Construction and Architectural Engineering **8** (6), 717-720 (2014).

[16] T. Aydin, M. Tarhan, B. Tarhan, J. Therm. An. Calori. **136**, 527-533 (2019).

[17] C.B. Ustundag, Y.K. Tur, A. Capoglu, J. Eur. Ceram. Soc. **26**, 169-177 (2006).

[18] G. Stathis, A. Ekonomakou, C.J. Stournaras, C. Ftikosa, J. Eur. Ceram. Soci. **24**, 2357-2366 (2004).

[19] M.O. Prado, E.D. Zanotto, C. Fredericci. http://www.lamav.ufscar.br/artpdf/procacers04.pdf

[20] M.O. Prado, E.D. Zanotto, C. Fredericci, Journal of Materials Research **18** [6], 1347 (2003).